Conductance spectroscopy of a correlated superconductor in a magnetic field in the Pauli limit: Evidence for strong correlations

Jan Kaczmarczyk* and Mariusz Sadzikowski†
Marian Smoluchowski Institute of Physics, Jagiellonian University, Reymonta 4, PL-30-059 Kraków, Poland

Jozef Spałek‡
Marian Smoluchowski Institute of Physics, Jagiellonian University, Reymonta 4, PL-30-059 Kraków, Poland and
Faculty of Physics and Applied Computer Science, AGH University of Science and Technology, Reymonta 19, PL-30-059 Kraków, Poland
(Received 1 June 2011; revised manuscript received 21 July 2011; published 26 September 2011)

We study conductance spectroscopy of a two-dimensional junction between a normal metal and a *strongly correlated* superconductor (SC) in an applied magnetic field in the Pauli limit. Depending on the field strength, the SC is either in the Bardeen-Cooper-Schrieffer (BCS) or in the Fulde-Ferrell-Larkin-Ovchinnikov (FFLO) state of the Fulde-Ferrell type. The strong correlations are accounted for by means of the Gutzwiller method, which naturally leads to the emergence of the spin-dependent masses of quasiparticles when the system is spin polarized. The case without strong correlations (with the spin-independent masses) is analyzed for comparison. We consider both the s-wave and the d-wave symmetries of the SC gap and concentrate on the parallel orientation of the Cooper-pair momentum $\mathbf{Q}$ with respect to the junction interface. The junction conductance is presented for selected barrier strengths (i.e., in the contact, the intermediate, and the tunneling limits). The conductance spectra in the cases with and without strong correlations differ essentially. Thus, our analysis provides an experimentally accessible *test for the presence of strong correlations in the SC state*. Namely, correlations alter the distance between the conductance peaks (or related conductance features) for carriers with spin up and spin down. In the uncorrelated case, this distance is twice the Zeeman energy. In the correlated case, the corresponding distance is about 30%–50% smaller, but other models may provide even stronger differences, depending on the details of the system's electronic structure. It turns out that the strong correlations manifest themselves most clearly in the case of the junction with the BCS, rather than the FFLO SC, what should make the experimental verification of the present results simpler.

DOI: 10.1103/PhysRevB.84.094525 PACS number(s): 74.45.+c, 71.27.+a, 71.10.Ca, 74.50.+r

I. INTRODUCTION

The search for evidence of strong electron correlations in condensed matter has concentrated in recent years on the superconducting (SC) state in unconventional materials and its coexistence with magnetism. One such example is the search for experimental evidence for the Fulde-Ferrell-Larkin-Ovchinnikov (FFLO) SC state. The FFLO state was proposed theoretically in the 1960s.[1,2] In this unconventional SC state, the Fermi wave-vector difference for the electrons with spin up and spin down due to the presence of the Zeeman term makes it favorable for the Cooper pair to acquire a nonzero total momentum $\mathbf{Q} = 2\mathbf{q}$. Consequently, the phase of the SC gap parameter oscillates spatially with the wave vector $\mathbf{Q}$. By forming such a condensate of moving Cooper pairs, the SC state persists for magnetic fields remarkably higher than the Pauli H_{c2} limit. Recently, the FFLO state suddenly gained renewed interest (for a review, see Ref. 3) because of its possible detection in the heavy-fermion SC $CeCoIn_5$,[4–7] although the nature of the high-field low-temperature phase observed in this system is still under intensive debate after antiferromagnetism was observed in the vicinity of this phase.[8–12] The FFLO state has also been proposed for κ-$(BEDT\text{-}TTF)_2Cu(NCS)_2$,[13,14] β''-$(ET)_2SF_5CH_2CF_2SO_3$,[15] and other layered organic SCs (see references in Ref. 14). Also, the existence of the FFLO state has been indicated in other heavy-fermion systems: $PuRhGa_5$,[16] Ce_2PdI_8,[17] (see Ref. 18, Sec. VB1 for a more detailed account), as well as in the pnictide SC LiFeAs.[19] The FFLO state has also been investigated in high-density quark and nuclear matter[20] as well as in optical lattices.[21–23]

All systems considered so far to be a host to the FFLO phase have a *reduced dimensionality*, which is crucial for the FFLO phase stability because then the orbital effects are suppressed and the Pauli effect (Zeeman splitting) may become the dominant factor. Another obvious feature, which suppresses the orbital effects, is the *heavy quasiparticle mass*. These characteristics of possible FFLO hosts indicate that these systems are *likely to have strong electron (fermion) correlations* and, thus, also possess specific features resulting from them.

The role of strong correlations in the most likely candidate for the FFLO state $CeCoIn_5$ is essential not only because this system is a heavy-fermion SC with very narrow bands originating from $4f$ electrons hybridized with $5d$-$6s$ states, but also, what is equally important is that the spin-dependent effective masses (SDMs) of quasiparticles have been observed directly in this system[24] by means of the de Haas–van Alphen oscillations in a strong applied magnetic field. SDMs are one of the hallmarks of strong correlations, as they appear naturally in theories incorporating correlations (Gutzwiller,[25] slave bosons,[26,27] dynamical mean-field theory,[28] and fluctuation-exchange approximation[29]), when the system is spin polarized.[30]

Because of the above reasons, it is important to study the effect of correlations on the FFLO phase. Such analysis has already been performed in a few cases,[31–35] and it indicates,

among other things, that the interelectronic correlations play an important role in forming and stabilizing the FFLO phase.

In the present paper, we concentrate on providing experimentally accessible concrete characteristics of a SC state with strong correlations. Namely, we study the conductance of a normal-metal-SC junction (NSJ) with the strongly correlated SC in either the Fulde-Ferrell (FF) type of the FFLO state or the Bardeen-Cooper-Schrieffer (BCS) state (the latter is stable in lower fields). Conductance spectroscopy of such a junction is an experiment sensitive to both the phase and the amplitude modulations of the SC order parameter, and therefore, it is a candidate technique for providing direct evidence for the presence of the FFLO phase. In that situation, a crucial role is played by the Andreev reflection (AR) processes.[36] In the simplest view of the AR, an incident electron entering from the normal metal into the SC is converted at the NSJ interface into a hole moving in the opposite direction (to the incident particle) and Cooper pair inside the SC. Such processes increase the conductance of the junction (in an ideal case by a factor of 2), which is analyzed in the framework provided by Blonder *et al.*[37]

The conductance characteristics for a NSJ with a SC in the FFLO state has already been investigated for both the cases of the FF [with $\Delta(\mathbf{r}) = \Delta_{\mathbf{Q}} e^{i\mathbf{Q}\mathbf{r}}$][38–40] and the Larkin-Ovchinnikov (LO) [$\Delta(\mathbf{r}) = \Delta_{\mathbf{Q}} \cos(\mathbf{Q}\mathbf{r})$][41] types of FFLO states as well as for the case of the SC with a supercurrent[42,43] (i.e., the situation similar to ours from a formal point of view). See also Refs. 44–47 for the case of a NSJ with a BCS state of the d-wave symmetry. None of the above papers have taken strong electron correlations into account.

Here, we consider both the cases of s-wave and d-wave strongly correlated SCs in a magnetic field and in the Pauli limiting situation (i.e., we neglect the orbital effects, as the Maki parameter[48] in the systems of interest, is quite high[5]). The strong correlations are taken into account by assuming dispersion relations with SDMs of quasiparticles and with the correlation field, as given, e.g., by the Gutzwiller approximation[25] or slave-boson theory.[26] The case without strong correlations [with spin-independent masses (SIMs)] is analyzed for comparison. In low magnetic fields, the SC is in the BCS state, and in higher magnetic fields, a transition to the FFLO state takes place. We only consider the simpler FF type of FFLO state as we intend to single out features of the situation with strong correlations in the simplest case (the analysis of the LO state is much more complex[41]). Our paper already leads to interesting results in this simplest situation. We set the direction of the Cooper-pair momentum $\mathbf{Q}$ as either perpendicular or parallel to the junction interface, with more attention paid to the latter situation. The analysis is performed in a fully self-consistent manner. Namely, we select Cooper-pair momentum $\mathbf{Q}$ minimizing the free energy of the system, and we determine the chemical potential μ in each phase separately so that the particle number n is kept constant. Such an adjustment of μ is required even for the BCS state for the narrow-band case. Also, such a careful examination of the SC properties is important, and non-self-consistent calculations may lead to important alterations of the conductance spectrum.[39]

As we deal with heavy quasiparticles on the SC side of the NSJ, in principle, we should take the Fermi-velocity-mismatch effects into account. Under those circumstances, the AR processes would be limited severely by a high effective barrier strength Z. On the other hand, AR is clearly observed in junctions with heavy-fermion superconductors,[49,50] and theoretical efforts have been made to understand why this is the case.[51–53] Based on these studies, we disregard the Fermi-velocity mismatch by assuming equal chemical potentials and equal *average* masses of quasiparticles on both sides of the junction. Namely, we choose masses on the normal side as m_{av}, and on the superconductor side, we have that $(m_\uparrow + m_\downarrow)/2 = m_{av}$, with $m_{av} = 100\, m_0$ (where m_0 is the electron mass in vacuum), which roughly corresponds to the band of heaviest quasiparticles for $CeCoIn_5$.[24] This assumption is, in our view, a justifiable simplification, as we would like to single out the features of the NSJ conductance in their clearest form. Note also, that we consider a model situation with its parameters taken from the experiment for $CeCoIn_5$.

In brief, we study the conductance of the NSJ with the SC exhibiting strong electron correlations (SDM case). To single out specific features of such a situation, we also study the uncorrelated case (SIM) and compare those results.

The paper is organized as follows. In Sec. II, we discuss the SC state of quasiparticles with SDMs and SIMs for a two-dimensional electron gas. In Sec. III, we present the theory concerning the conductance of a normal-metal strongly correlated SC junction. In Sec. IV, we show conductance spectra for the cases with SDMs and SIMs. In Sec. V, we discuss the relation of our results to experiments and suggest their possible experimental verification. Finally, in Sec. VI, we provide a brief summary.

II. FF SC STATE BASIC CHARACTERISTICS: MODEL AND METHOD

As said above, here we consider a two-dimensional system of paired quasiparticles in the situations with SDMs and SIMs. The system of self-consistent equations describing such a SC state has already been presented in detail in Refs. 31 and 32. For the sake of completeness, here, we provide a brief summary of our procedure. We start with the Hamiltonian,

$$\hat{\mathcal{H}} = \sum_{\mathbf{k}\sigma} \xi_{\mathbf{k}\sigma} a^\dagger_{\mathbf{k}\sigma} a_{\mathbf{k}\sigma} + \frac{1}{N} \sum_{\mathbf{k}\mathbf{k}'\mathbf{q}} V_{\mathbf{k},\mathbf{k}'} a^\dagger_{\mathbf{k}+\mathbf{q}\uparrow} a^\dagger_{-\mathbf{k}+\mathbf{q}\downarrow} a_{-\mathbf{k}'+\mathbf{q}\downarrow} a_{\mathbf{k}'+\mathbf{q}\uparrow} + \frac{N}{n} \overline{m} h_{\mathrm{cor}}, \tag{1}$$

where $\mathbf{Q} = 2\mathbf{q}$ is the wave vector of the Cooper-pair center of mass, $n \equiv n_\uparrow + n_\downarrow$ is the band filling, $\overline{m} \equiv n_\uparrow - n_\downarrow$ is the spin polarization of the system, and N is the total number of particles. The dispersion relation for the cases with SDMs and SIMs is chosen, respectively, as

$$\xi_{\mathbf{k}\sigma} = \frac{\hbar^2 k^2}{2m_\sigma} - \sigma(h + h_{\mathrm{cor}}) - \mu, \tag{2}$$

$$\xi^{(\mathrm{SIM})}_{\mathbf{k}\sigma} = \frac{\hbar^2 k^2}{2m_{av}} - \sigma h - \mu, \tag{3}$$

where $h \equiv g\mu_B H/2$, with H being the applied magnetic field. The quantity h_{cor} is the correlation field that appears naturally in both the slave-boson theory (it is equivalent to $-\beta$ of Ref. 26) and the Gutzwiller approximation if this approximation is

performed with care.[54–56] Justification of a Hamiltonian with both the pairing part and the SDM can be found in Ref. 33 (Appendix A) and in Ref. 57. The spin-dependent quasiparticle mass is equal to $m_\sigma \equiv m_B/q_\sigma(n,\overline{m})$, where m_B is the bare-band mass and $q_\sigma(n,\overline{m})$ is the band-narrowing factor. Explicitly (in the Hubbard $U \to \infty$ limit), the quasiparticle masses are given by[25,26]

$$\frac{m_\sigma}{m_B} = \frac{1-n_\sigma}{1-n} = \frac{1-n/2}{1-n} - \sigma\,\frac{\overline{m}}{2(1-n)} \equiv \frac{1}{m_B}(m_{av} - \sigma\,\Delta m/2), \tag{4}$$

with $\Delta m \equiv m_\downarrow - m_\uparrow$ (note that $\sigma = \uparrow$ labels the spin-majority subband). Next, as in the BCS theory, we take the pairing potential in a separable form and assume it is nonzero in a small region around the Fermi surface (for details, see Refs. 31, 32, and 58),

$$V_{\mathbf{k},\mathbf{k}'} = -V_0\eta_\mathbf{k}\eta_{\mathbf{k}'}, \tag{5}$$

where $\eta_\mathbf{k} \equiv \cos(a_0k_x) - \cos(a_0k_y)$ for the d-wave case [with $a_0 = 4.62$ Å being the lattice constant for $CeCoIn_5$ (Ref. 59)] and $\eta_\mathbf{k} \equiv 1$ for the s-wave case. Under such assumptions, the SC gap can be factorized as

$$\Delta_{\mathbf{k},\mathbf{Q}} = \Delta_\mathbf{Q}\eta_\mathbf{k}. \tag{6}$$

Following the standard mean-field approach to Hamiltonian (1), we obtain the generalized free-energy functional $\mathcal{F}$ and the system of self-consistent equations as follows[31,32]:

$$\mathcal{F} = -k_BT\sum_{\mathbf{k}\sigma}\ln(1+e^{-\beta E_{\mathbf{k}\sigma}}) + \sum_\mathbf{k}\left(\xi^{(s)}_\mathbf{k} - E_\mathbf{k}\right) + N\frac{\Delta^2_\mathbf{Q}}{V_0} + \mu N + \frac{N}{n}\overline{m}h_{\rm cor}, \tag{7}$$

$$h_{\rm cor} = -\frac{n}{N}\sum_{\mathbf{k}\sigma}f(E_{\mathbf{k}\sigma})\frac{\partial E_{\mathbf{k}\sigma}}{\partial\overline{m}} + \frac{n}{N}\sum_\mathbf{k}\frac{\partial\xi^{(s)}_\mathbf{k}}{\partial\overline{m}}\left(1-\frac{\xi^{(s)}_\mathbf{k}}{E_\mathbf{k}}\right), \tag{8}$$

$$\overline{m} = \frac{n}{N}\sum_{\mathbf{k}\sigma}\sigma f(E_{\mathbf{k}\sigma}), \tag{9}$$

$$\Delta_\mathbf{Q} = \frac{V_0}{N}\sum_\mathbf{k}\eta^2_\mathbf{k}\frac{1-f(E_{\mathbf{k}\uparrow})-f(E_{\mathbf{k}\downarrow})}{2E_\mathbf{k}}\Delta_\mathbf{Q}, \tag{10}$$

$$n = n_\uparrow + n_\downarrow = \frac{n}{N}\sum_{\mathbf{k}\sigma}\left\{u^2_\mathbf{k}f(E_{\mathbf{k}\sigma}) + v^2_\mathbf{k}[1-f(E_{\mathbf{k},-\sigma})]\right\}, \tag{11}$$

where $\mathcal{F}(T,H,\mu;\overline{m},h_{\rm cor},\Delta_\mathbf{Q},n)$ is the system free-energy functional for the case of a fixed number of particles[23] (we fix the band filling at the value $n = 0.97$), V_0 is the interaction potential, $u_\mathbf{k}$, $v_\mathbf{k}$ are the Bogoliubov coherence coefficients, $f(E_{\mathbf{k}\sigma})$ is the Fermi distribution, and n_σ is the spin-sub-band filling. The physical solution is the one with a particular $\mathbf{Q}$ that minimizes the free energy F, which, in turn, is obtained from $\mathcal{F}$ by evaluating the latter at the values of parameters, which are the solution to Eqs. (8)–(11). The state with $\mathbf{Q} = 0$ is called the BCS state, and that with $\mathbf{Q} \neq 0$ is called the FF state.

TABLE I. Equilibrium values of mean-field variables and related quantities for the s-wave solution with $H = 10.01$ T and $T = 0.02$ K.

Variable	Value	Variable	Value
$\overline{m}$	0.012 9431	Δm (m_0)	2.513 22
$h_{\rm cor}$ (K)	−3.082 30	$h_{\rm cor\,NS}$ (K)	−3.265 46
$\Delta_\mathbf{Q}$ (K)	1.389 22	$\lvert\mathbf{Q}\rvert$ (Å^{-1})	0.009 47
μ (K)	126.287	$\lvert\mathbf{Q}\rvert/\Delta k_F$	1.08
F (K)	61.182 002 88	ΔF (K) $\equiv F_{\rm NS} - F$	−0.001 113 51

The quasiparticle spectrum in the paired state is characterized by the energies (cf. also Ref. 60),

$$E_{\mathbf{k}\sigma} \equiv E_\mathbf{k} + \sigma\xi^{(a)}_\mathbf{k}, \quad E_\mathbf{k} \equiv \sqrt{\xi^{(s)2}_\mathbf{k} + |\Delta_{\mathbf{k},\mathbf{Q}}|^2}, \tag{12}$$

$$\xi^{(s)}_\mathbf{k} \equiv \tfrac{1}{2}(\xi_{\mathbf{k}+\mathbf{q}\uparrow} + \xi_{-\mathbf{k}+\mathbf{q}\downarrow}), \quad \xi^{(a)}_\mathbf{k} \equiv \tfrac{1}{2}(\xi_{\mathbf{k}+\mathbf{q}\uparrow} - \xi_{-\mathbf{k}+\mathbf{q}\downarrow}). \tag{13}$$

Equations (8)–(11) are solved by numerical integration over the reciprocal space. We use procedures from the GNU Scientific Library[61] as solvers. For the SIM case, $h_{\rm cor} = 0$, and we only solve Eqs. (9)–(11). The numerical procedure has been elaborated in detail elsewhere.[58] Here, for completeness, in Tables I and II, we also provide the numerical values of selected parameters for the situations with the s-wave and the d-wave symmetries of the SC gap, respectively. The quantity $F_{\rm NS}$ is the free energy of the normal state (NS), and therefore, ΔF is the condensation energy. Also, $\Delta m \equiv m_2 - m_1$ is the mass difference and $h_{\rm cor\,NS}$ is the correlation field value in the NS. The free energies are calculated per elementary cell. The numerical accuracy is not smaller than on the level of the last digit specified.

The input parameters in our method have the following values: the band filling $n = 0.97$, the lattice constant $a_0 = 4.62$ Å, the interaction potential strength $V_0/n = 90$ K (d wave) and $V_0/n = 110$ K (s wave), the interaction potential width (cutoff) $\hbar\omega_C = 17$ K, and the quasiparticle average mass $m_{av} = 100\,m_0$. The other parameters (in particular, $\overline{m}$, $h_{\rm cor}$, $\Delta_\mathbf{Q}$, μ, $\mathbf{Q}$, and $\theta_\mathbf{Q}$) are determined from the solution procedure.

Exemplary phase diagrams obtained on the applied field H and temperature T plane are exhibited in Figs. 1 and 2 for the s-wave and the d-wave cases, respectively. The angle $\theta_\mathbf{Q}$ is the angle between the maximum-gap (antinodal) direction and the Cooper-pair momentum $\mathbf{Q}$. Note that, in both situations, the FF state is more robust (i.e., the FF state fills a wider field-temperature range on the phase diagram) in the SDM case than in the SIM case. The mechanism of the FF-state

TABLE II. Equilibrium values of mean-field variables and related quantities for the d-wave solution with $H = 20.01$ T and $T = 0.1$ K.

Variable	Value	Variable	Value
$\overline{m}$	0.026 8690	Δm (m_0)	5.217 29
$h_{\rm cor}$ (K)	−6.408 70	$h_{\rm cor\,NS}$ (K)	−6.531 33
$\Delta_\mathbf{Q}$ (K)	1.274 55	$\lvert\mathbf{Q}\rvert$ (Å^{-1})	0.0183
μ (K)	126.416	$\lvert\mathbf{Q}\rvert/\Delta k_F$	1.15
F (K)	61.043 421 25	ΔF (K) $\equiv F_{\rm NS} - F$	−0.001 424 36

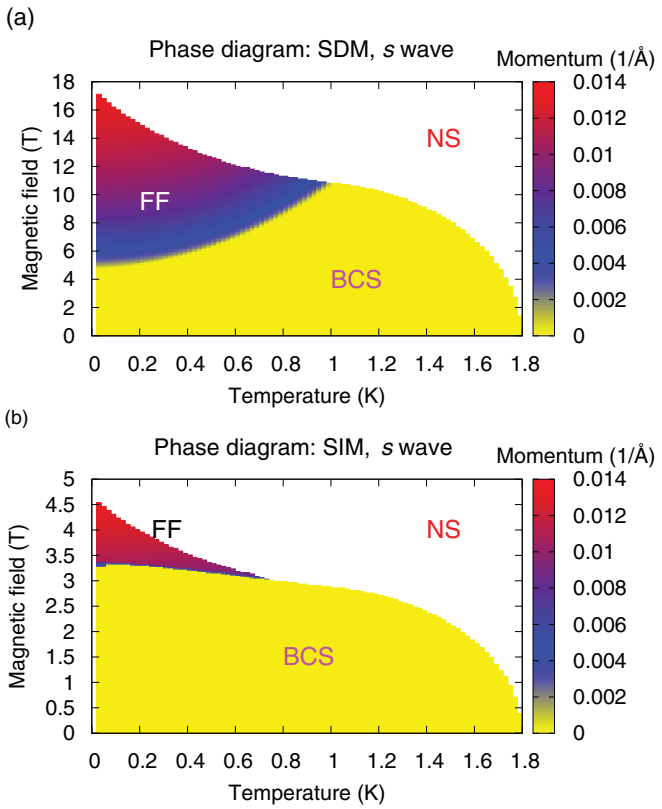

FIG. 1. (Color online) Phase diagram for the s-wave gap symmetry in the (a) SDM and (b) SIM cases. Light (yellow) region corresponds to $\mathbf{Q} = 0$ (BCS phase), the darker region corresponds to the state with $\mathbf{Q} \neq 0$ (FF phase), and the white region corresponds to the NS. Note the greater difference between SDM and SIM cases than for d-wave gap symmetry (see Fig. 2).

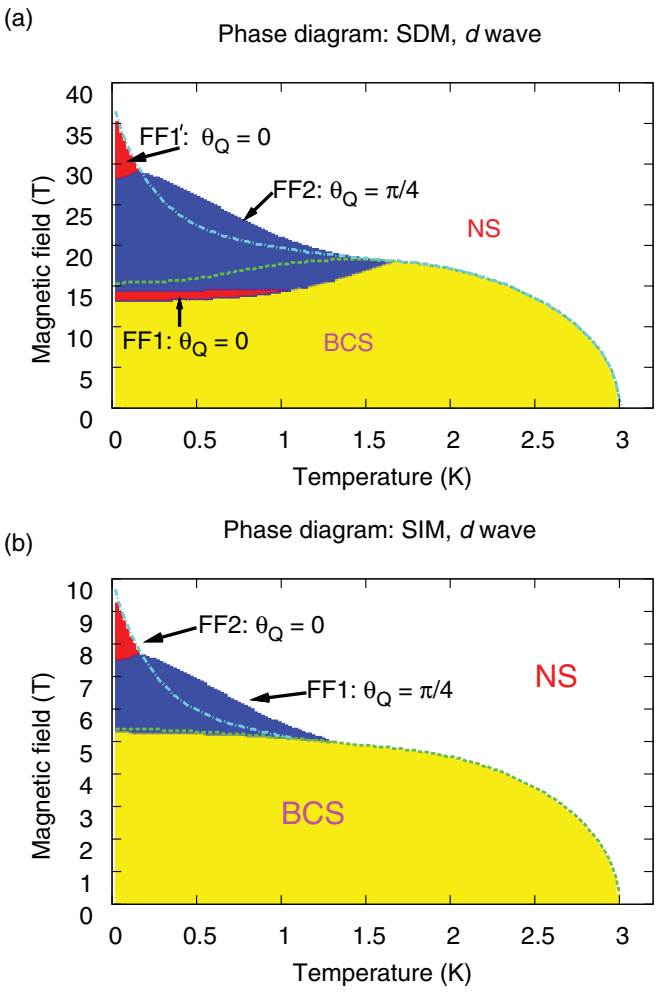

FIG. 2. (Color online) Phase diagram for the d-wave gap symmetry for the cases with (a) SDM and (b) SIM. Light (yellow) region corresponds to $\mathbf{Q} = 0$ (BCS phase), the darker (blue, red) region corresponds to the states with $\mathbf{Q} \neq 0$ (FF phases), and the white region corresponds to the NS. The topmost (red) region [and FF1 region in (a)] corresponds to the Cooper-pair momentum $\mathbf{Q}$ in the maximum-gap (antinodal) direction ($\theta_{\mathbf{Q}} = 0$), whereas, the middle one (blue) corresponds to the momentum along the nodal direction ($\theta_{\mathbf{Q}} = \pi/4$). Note that this anisotropy results solely from the d-wave gap symmetry, as the unpaired gas is isotropic. The dashed line marks the BCS critical field H_{c2} in the Pauli limit, and the dot-dashed line marks H_{c2} for the solution with $\theta_{\mathbf{Q}} = 0$.

stabilization by strong correlations has been analyzed in detail in Refs. 31–33. For the sake of completeness, let us mention that this mechanism is based on a smaller Fermi-wave-vector splitting ($\Delta k_F \equiv k_{F\uparrow} - k_{F\downarrow}$) in the SDM situation. In such a case, the system can resist the destabilizing influence of the applied magnetic field (hence, higher critical fields in the SDM case) more efficiently. Also, it turns out that the FF state can benefit to a greater extent than the BCS state from the smaller Δk_F, as the FF state has higher spin polarization, which is necessary for the appearance of SDMs (for details, see Refs. 31, 32, and 58).

For further analysis of the AR, we take the parameters obtained along the $T = 0.02$ K ≈ 0 line in Figs. 1 and 2. Therefore, the results will have, strictly speaking, practical relevance for $T \ll T_{sc}$, with the SC transition temperature $T_{sc} \approx 2$ to 3 K, as can be seen from Figs. 1 and 2.

III. JUNCTION CONDUCTANCE: THEORETICAL ANALYSIS

For the analysis of the NSJ conductance, we take the SC state parameters obtained self-consistently (from the procedure presented above). Here, we consider only two-dimensional NSJ for simplicity. Kinematics of the reflection may be analyzed by means of the Bogoliubov–de Gennes (BdG) equations,[62]

$$E u_\sigma(\mathbf{x}) = \hat{\mathcal{H}}_0 u_\sigma(\mathbf{x}) + \int d\mathbf{x}' \Delta(\mathbf{s},\mathbf{r}) v_\sigma(\mathbf{x}'), \tag{14}$$

$$E v_\sigma(\mathbf{x}) = -\hat{\mathcal{H}}_0 v_\sigma(\mathbf{x}) + \int d\mathbf{x}' \Delta^*(\mathbf{s},\mathbf{r}) u_\sigma(\mathbf{x}'), \tag{15}$$

where $\mathbf{s} = \mathbf{x} - \mathbf{x}'$, $\mathbf{r} = (\mathbf{x} + \mathbf{x}')/2$, and $\sigma = \pm 1$ is the spin quantum number of the incoming quasiparticle and $u_\sigma(\mathbf{x})$ and $v_\sigma(\mathbf{x})$ are the particle and hole wave-function components. The one-particle Hamiltonian is given by

$$\hat{\mathcal{H}}_0(\mathbf{r}) = -\nabla \frac{\hbar^2}{2\, m(\mathbf{r})} \nabla - \sigma h - \sigma h_{\mathrm{cor}}(\mathbf{r}) - \mu + V(\mathbf{r}), \tag{16}$$

where we have used the effective-mass approximation[63,64] to express the kinetic part as $\nabla \frac{\hbar^2}{2\,m(x)} \nabla$ with $m(\mathbf{r}) \equiv m(x) = m_{av}\Theta(-x) + m_\sigma \Theta(x)$, similar to Refs. 64–67. The correlation field is nonzero only on the SC side of the junction [$h_{\rm cor}(\mathbf{r}) = h_{\rm cor}\Theta(x)$]. Also, $\mathbf{r} = (x, y)$, and the interface scattering potential is chosen as a δ function of strength $\tilde{H}$, i.e., $V(\mathbf{r}) = \tilde{H}\delta(x)$. The gap function can be Fourier transformed as follows:

$$\Delta(\mathbf{s},\mathbf{r}) = \int d\mathbf{k}\, e^{i\mathbf{k}\mathbf{s}} \tilde{\Delta}(\mathbf{k},\mathbf{r}) = \int d\mathbf{k}\, e^{i\mathbf{k}\mathbf{s}} \Delta_{\mathbf{k},\mathbf{Q}} e^{i\mathbf{Q}\mathbf{r}}\, \Theta(x), \tag{17}$$

with $\Delta_{\mathbf{k},\mathbf{Q}}$ as in Eq. (6) but with the original set of coordinates rotated by α (cf. Fig. 3). Explicitly, the SC gap we use from now on has the form (in the new coordinates)

$$\begin{aligned}\Delta_{\mathbf{k},\mathbf{Q}} = \Delta_{\mathbf{Q}} [&\cos(a_0 k_x \cos\alpha - a_0 k_y \sin\alpha) \\ &- \cos(a_0 k_y \cos\alpha + a_0 k_x \sin\alpha)].\end{aligned} \tag{18}$$

We neglect the proximity effects by assuming a steplike gap function. To solve the BdG equations, we make the plane-wave ansatz. Namely, we assume that the two-component pair wave function has the form

$$\psi(\mathbf{r},\sigma) \equiv \begin{bmatrix} u_\sigma(\mathbf{r})|\sigma\rangle \\ v_\sigma(\mathbf{r})|\overline{\sigma}\rangle \end{bmatrix} = e^{i\mathbf{k}\mathbf{r}} \begin{bmatrix} \tilde{u} e^{i\mathbf{q}\mathbf{r}}|\sigma\rangle \\ \tilde{v} e^{-i\mathbf{q}\mathbf{r}}|\overline{\sigma}\rangle \end{bmatrix}, \tag{19}$$

with $\tilde{u}$ and $\tilde{v}$ as constants and with $\overline{\sigma} \equiv -\sigma$ (we have also dropped the σ indices of $\tilde{u}$ and $\tilde{v}$). We also remind the reader that $\mathbf{q} = \mathbf{Q}/2$. By substituting Eqs. (17) and (19) into BdG equations (14) and (15) and after some algebra, we obtain the following matrix equation:

$$\begin{pmatrix} -E + \xi_{\mathbf{k}+\mathbf{q},\sigma} & \Delta_{\mathbf{k},\mathbf{Q}} \\ \Delta^*_{-\mathbf{k},\mathbf{Q}} & -E - \xi_{\mathbf{k}-\mathbf{q},\overline{\sigma}} \end{pmatrix} \begin{pmatrix} \tilde{u}|\sigma\rangle \\ \tilde{v}|\overline{\sigma}\rangle \end{pmatrix} = 0, \tag{20}$$

where unpaired quasiparticle energies $\xi_{\mathbf{k}\sigma}$ are given by Eq. (2) or (3). Equation (20) gives the dispersion relations for quasiparticles and quasiholes in the SC,

$$E = E_{\mathbf{k}\pm} = \begin{cases} \xi^{(a)}_{\mathbf{k}} \pm \sqrt{\xi^{(s)2}_{\mathbf{k}} + \Delta_{\mathbf{k},\mathbf{Q}} \Delta^*_{-\mathbf{k},\mathbf{Q}}} & \text{for } \sigma = \uparrow, \\ -\xi^{(a)}_{-\mathbf{k}} \pm \sqrt{\xi^{(s)2}_{-\mathbf{k}} + \Delta_{\mathbf{k},\mathbf{Q}} \Delta^*_{-\mathbf{k},\mathbf{Q}}} & \text{for } \sigma = \downarrow, \end{cases} \tag{21}$$

where $\xi^{(s,a)}_{\mathbf{k}}$ have been defined in Eq. (13). One may check that the above equation is in accordance with Eq. (12), as $E_{\mathbf{k}+} = E_{\mathbf{k}\uparrow}$ (quasiparticle) and $E_{\mathbf{k}-} = -E_{\mathbf{k}\downarrow}$ (quasihole) for an incoming particle with spin $\sigma = \uparrow$ as well as $E_{\mathbf{k}+} = E_{-\mathbf{k}\downarrow}$ (quasiparticle) and $E_{\mathbf{k}-} = -E_{-\mathbf{k}\uparrow}$ (quasihole) for an incoming particle with spin $\sigma = \downarrow$. This holds as long as $\Delta^*_{-\mathbf{k},\mathbf{Q}} = \Delta^*_{\mathbf{k},\mathbf{Q}}$, which is true for any real $\mathbf{k}$.

As already mentioned, we study the FF type of the FFLO SC state in which $\Delta(\mathbf{r}) = \Delta_{\mathbf{Q}} e^{i2\mathbf{q}\mathbf{r}}$ and set the direction of the Cooper-pair momentum $\mathbf{Q} = 2\mathbf{q}$ as either perpendicular [$\mathbf{Q} = (Q,0)$] or parallel [$\mathbf{Q} = (0,Q)$] to the junction interface. The perpendicular configuration [$\mathbf{Q} = (Q,0)$] may lead to an accumulation of charge at the NSJ interface due to normal and/or supercurrents present in the FF state. Therefore, we pay principal attention to the parallel configuration. Parenthetically, the accumulation processes are very slow for the case of heavy quasiparticles.

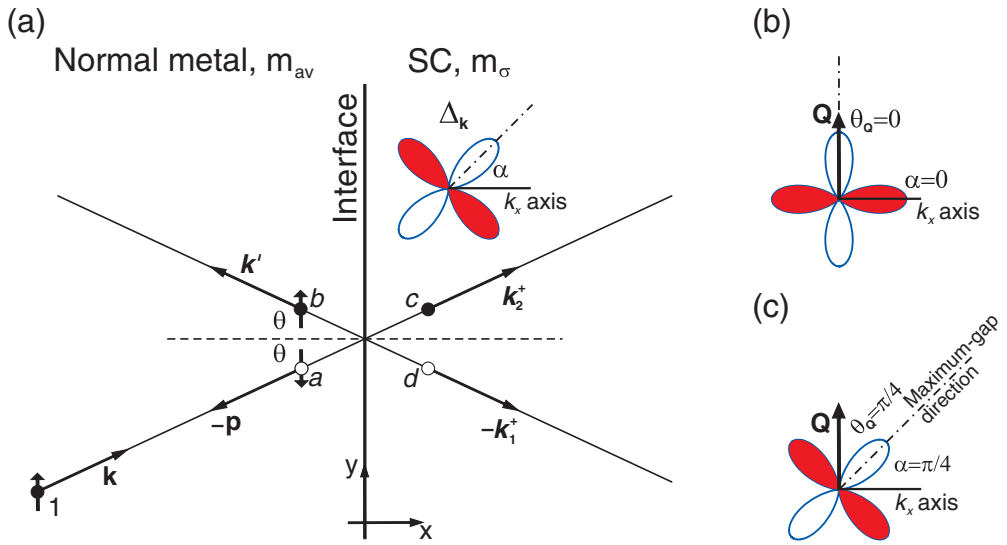

FIG. 3. (Color online) (a) Junction geometry for an incoming particle of spin $\sigma = \uparrow$. Normal metal and SC regions are marked. The interface lies at the $x = 0$ line. The SC gap is also presented: α is the angle between the k_x axis and the maximum-gap direction. The full circles mark quasiparticles, and the empty ones mark quasiholes. The momentum of each of them is marked with a boldface letter, and the amplitude is marked with an italic letter. Namely, the incoming particle has momentum $\mathbf{k}$ and amplitude 1, the reflected hole has momentum $\mathbf{p}$ and amplitude a, the reflected quasiparticle has momentum $\mathbf{k}'$ and amplitude b, the transmitted quasiparticle has momentum $\mathbf{k}_2^+$ and amplitude c, and the transmitted quasihole has momentum $\mathbf{k}_1^+$ and amplitude d. Note that the velocities of (quasi)holes are in the opposite direction to their momenta. The angle of incidence is equal to θ and to the angle of reflection, but other angles (of reflection of the hole and those of transmissions) may differ (cf. also Fig. 4). In (b) and (c), we explicitly show the two d-wave configurations of the SC gap for the FF phase studied in the following: (b) corresponds to Fig. 7, and (c) corresponds to Fig. 8.

As we consider an electron injected from the conductor side of the junction (junction geometry is presented in Fig. 3), the corresponding wave functions can be expressed as (we have omitted the spin part for clarity)

$$\psi_<(\mathbf{r}) = \begin{pmatrix}1\\0\end{pmatrix} e^{i\mathbf{k}\mathbf{r}} + a\begin{pmatrix}0\\1\end{pmatrix} e^{i\mathbf{p}\mathbf{r}} + b\begin{pmatrix}1\\0\end{pmatrix} e^{i\mathbf{k}'\mathbf{r}}, \quad (22)$$

$$\psi_>(\mathbf{r}) = d\begin{pmatrix}u_1 e^{iq_x x}\\ v_1 e^{-iq_x x}\end{pmatrix} e^{i\mathbf{k}_1^+\mathbf{r}} + c\begin{pmatrix}u_2 e^{iq_x x}\\ v_2 e^{-iq_x x}\end{pmatrix} e^{i\mathbf{k}_2^+\mathbf{r}}, \quad (23)$$

where $\psi_<(\mathbf{r})$ and $\psi_>(\mathbf{r})$ describe the wave function on the normal-metal and SC sides, respectively. The quasimomenta $\mathbf{k}_1^+$ (for the quasihole) and $\mathbf{k}_2^+$ (for the quasiparticle) are solutions of Eq. (21) for a given incident energy E propagating in the positive x direction. From the translational symmetry of the junction along the y direction comes conservation of the y-momentum component. Namely, $k_y = k'_y = p_y = k_{1y}^+ = k_{2y}^+$. All the wave vectors are presented in Fig. 4.

We use boundary conditions with the appropriate masses[68] and the interface potential jump $\tilde{H}$; they are as follows:

$$\psi_<(\mathbf{r})|_{x=0} = \psi_>(\mathbf{r})|_{x=0}, \quad (24)$$

$$\frac{1}{m_{av}}\frac{\partial\psi_<(\mathbf{r})}{\partial x}\bigg|_{x=0} = \frac{1}{m_\sigma}\frac{\partial\psi_>(\mathbf{r})}{\partial x}\bigg|_{x=0} - \frac{2\tilde{H}}{\hbar^2}\psi_<(\mathbf{r})\bigg|_{x=0}. \quad (25)$$

Those conditions lead to the following set of four equations[69] for the amplitudes (a,b,c,d),

$$1 + b - cu_2 - du_1 = 0, \quad (26)$$

$$a - cv_2 - dv_1 = 0, \quad (27)$$

$$\frac{ik_x(1-b)}{m_{av}} - \frac{cu_2 i(q_x + k_{2x}^+)}{m_\sigma} - \frac{du_1 i(q_x + k_{1x}^+)}{m_\sigma} + \frac{2\tilde{H}}{\hbar^2}(1+b) = 0, \quad (28)$$

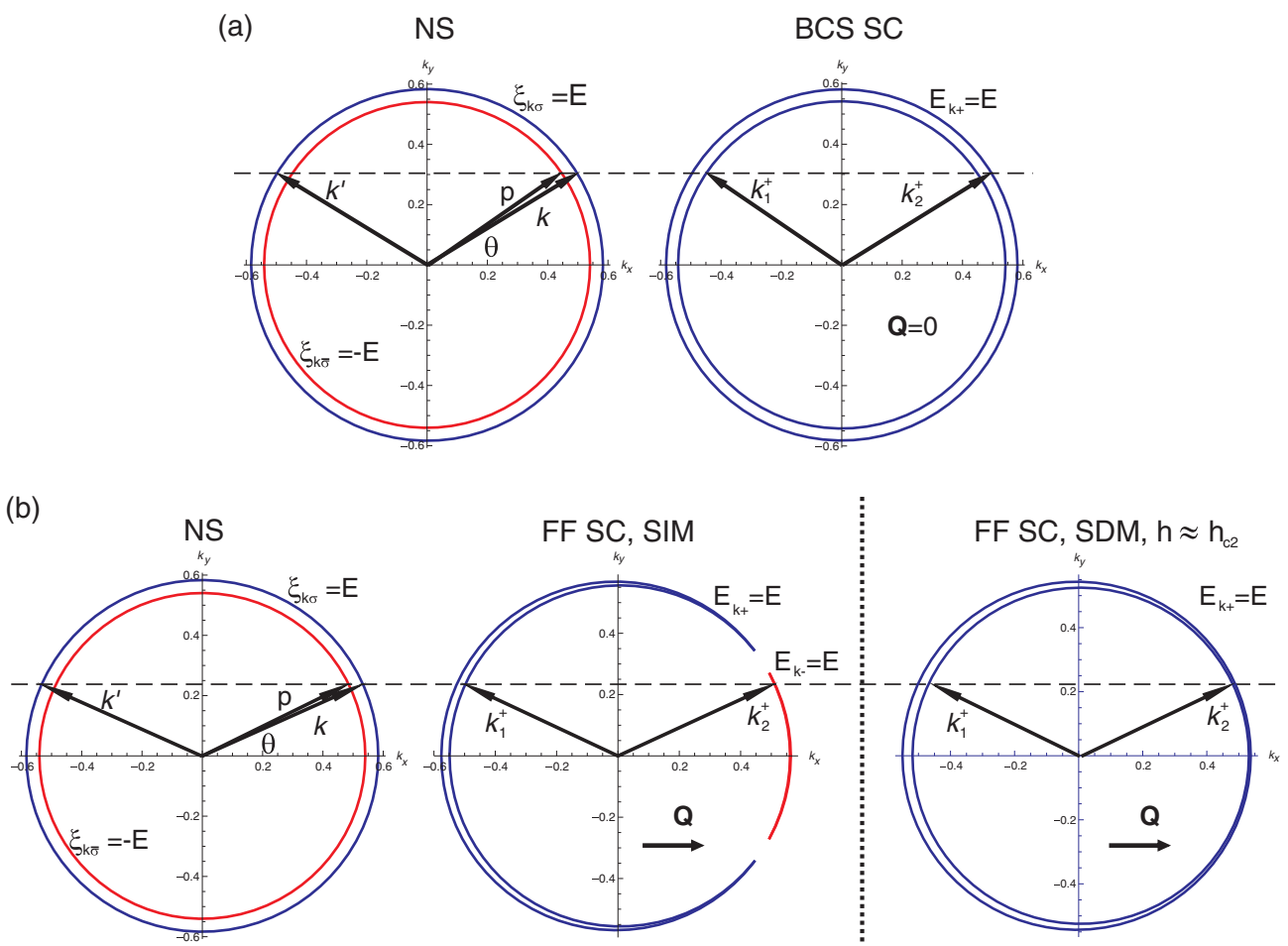

FIG. 4. (Color online) The junction geometry in reciprocal space. All relevant vectors are marked. It can be seen that only the incident and reflection angles are equal to θ. At this point, it can be anticipated that changing θ for the BCS state does not lead to drastic changes in the transmission/reflection probabilities, whereas, for the FF state, the situation is quite different, since $\mathbf{Q} \neq 0$ induces anisotropy in the reciprocal space. The energy E value has been chosen as 10 K for all graphs except (b) FF SC for which $E = 0.01$ K ≈ 0 (for $E > 0.5$ K, there would be no $E = E_{\mathbf{k}_-}$ regions in this case). The dashed lines are guides to eye and illustrate the conservation of the y-momentum component.

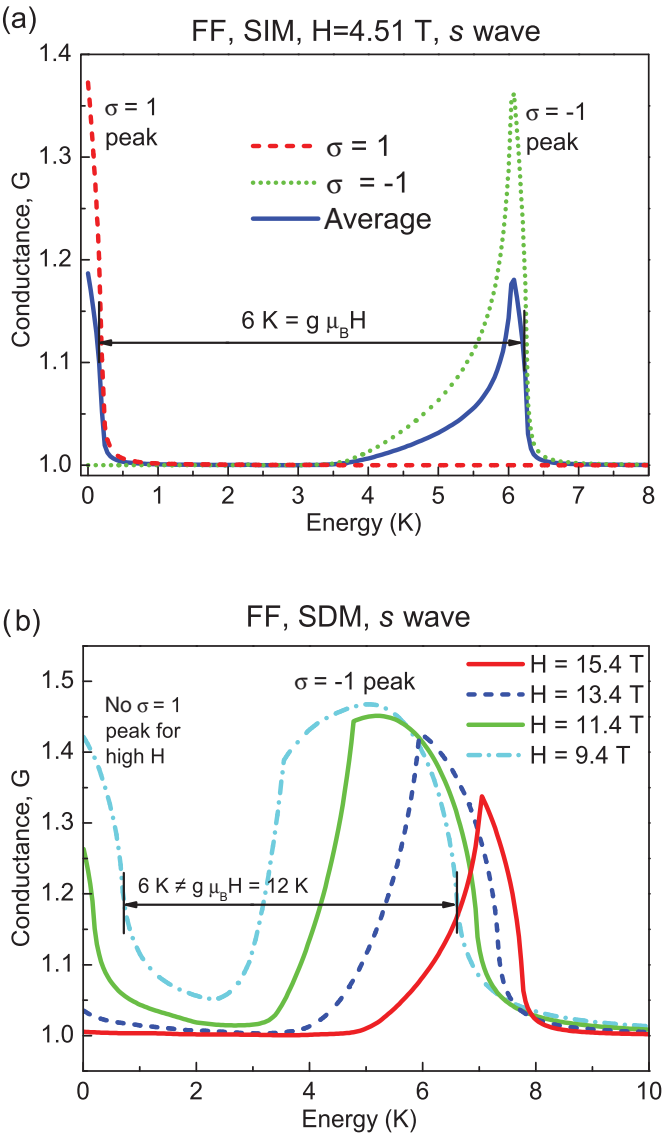

FIG. 5. (Color online) Conductance spectra for the case of s-wave FF states for (a) SIM and (b) SDM cases. The $\mathbf{Q}$ vector is oriented perpendicular to the junction, and the intermediate barrier strength $Z = 0.5$ is taken. The value of the gap is (a) $\Delta_{\mathbf{Q}} = 0.11$ K; (b) $\Delta_{\mathbf{Q}} =$ 0.36, 0.70, 1.09, and 1.53 K for the decreasing magnetic field. The distance between the peaks is twice the Zeeman energy $2h = g\mu_B H$ only for the SIM case. In the SDM case, the correlations compensate the Zeeman splitting (by means of $h_{\rm cor}$ and m_σ), and the peaks are closer than $g\mu_B H$.

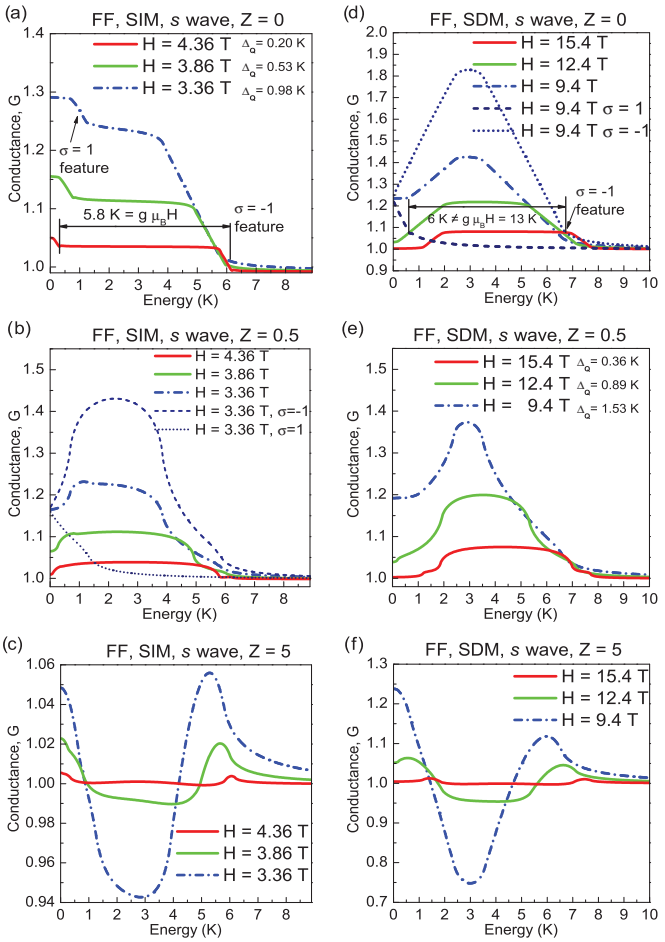

FIG. 6. (Color online) Conductance spectra for the case of the s-wave FF state for (a)–(c) SIMs and (d)–(f) SDMs, the $\mathbf{Q}$ vector oriented parallel to the junction, and selected Z values. Also, in (b) and (d), the spin-resolved signals G_σ are presented. The distance between the characteristic features is shown in (a) and (d). In (a) and (e), we provide the values of the gap $\Delta_{\mathbf{Q}}$ [they are identical in (a)–(c) and (d)–(f)]. In the SDM case, for $H \gtrsim 12$ T, there are no features of the spin-up signal because the junction is transparent for incoming electrons with spin $\sigma =\uparrow$ (for an explanation, see the main text).

$$\frac{aip_x}{m_{av}} - \frac{cv_2 i(k_{2x}^+ - q_x)}{m_{\bar\sigma}} - \frac{dv_1 i(k_{1x}^+ - q_x)}{m_{\bar\sigma}} + \frac{2\tilde H}{\hbar^2}a = 0, \tag{29}$$

which are similar to those in, e.g., Ref. 64, except in our case, vectors are replaced by their x components, e.g., $k \leftrightarrow k_x$, $p \leftrightarrow p_x$, and SDMs are properly accounted for (obviously, in the SIM case, we have that $m_\uparrow = m_\downarrow = m_{av}$). From the solution of Eqs. (26)–(29), one can obtain probabilities of the hole reflection $p_{rh}^\sigma = |a|^2 \frac{{\rm Re}[p_x]}{k_x}$, the particle reflection $p_{re}^\sigma = |b|^2$, the quasiparticle transmission,

$$p_{te}^\sigma = |c|^2 m_{av} \frac{\left(\frac{|u_2|^2}{m_\sigma} - \frac{|v_2|^2}{m_{\bar\sigma}}\right){\rm Re}[k_{2x}^+] + \left(\frac{|u_2|^2}{m_\sigma} + \frac{|v_2|^2}{m_{\bar\sigma}}\right)q_x}{k_x}, \tag{30}$$

and the quasihole transmission,

$$p_{th}^\sigma = |d|^2 m_{av} \frac{\left(\frac{|u_1|^2}{m_\sigma} - \frac{|v_1|^2}{m_{\bar\sigma}}\right){\rm Re}[k_{1x}^+] + \left(\frac{|u_1|^2}{m_\sigma} + \frac{|v_1|^2}{m_{\bar\sigma}}\right)q_x}{k_x}, \tag{31}$$

where the σ superscript indicates the spin of the incoming electron. In the following, we use the dimensionless barrier strength $Z \equiv 2m_{av}\tilde H/(k_F\hbar^2)$, where we define the Fermi wave vector k_F using the zero-field value $k_F = \frac{1}{\hbar}\sqrt{2m_{av}\mu}$. Note

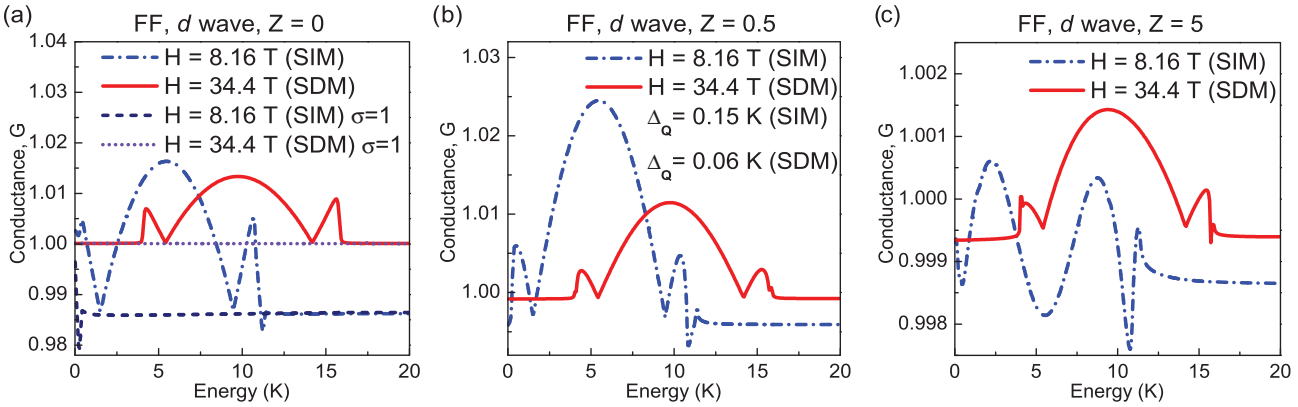

FIG. 7. (Color online) Conductance spectra for the case of the d-wave FF state for selected Z values for the SIM and SDM cases. The Cooper-pair momentum is oriented along the maximum-gap (antinodal) direction [i.e., $\theta_{\mathbf{Q}} = 0$ and $\alpha = 0$; cf. Figs. 2(a) and 3(b)]. In (b), we provide the values of the gap $\Delta_{\mathbf{Q}}$, and in (a), we also plot the spin-up conductance. The magnetic field is close to H_{c2}. There is no clear distinct feature, which differentiates between the SIM and the SDM situations for this configuration.

also that we do not use the assumption $k = k' = p = k_1^+ = k_2^+ \approx k_F$ utilized at this point in a majority of the papers on AR spectroscopy because we deal with heavy quasiparticles for which μ is on the order of 100 K. Therefore, the usual assumption $\mu \gg E$ is not, strictly speaking, applicable in the present situation.

IV. RESULTS AND PHYSICAL DISCUSSION

Differential conductance ($G \equiv dI/dV$) can be obtained from the reflection and transmission probabilities[37,70] in a straightforward manner,

$$G_{ns}^{\sigma} = \frac{1}{2}\int_{-\pi/2}^{\pi/2} d\theta \, \cos\theta \left[1 - p_{re}^{\sigma}(E,\theta) + p_{rh}^{\sigma}(E,\theta)\right]. \quad (32)$$

The final result of our calculation is the total conductance G averaged over spin and normalized with respect to the conductance G_{nn}^{σ} of the junction with $\Delta = 0$ but still with the same other parameters ($m_{\sigma}, \mu, h_{\mathrm{cor}}$), as the superconducting state. Namely,

$$G = \frac{G_{ns}^{\uparrow} + G_{ns}^{\downarrow}}{G_{nn}^{\uparrow} + G_{nn}^{\downarrow}}. \quad (33)$$

This quantity is exhibited in the following figures, sometimes with the spin-resolved conductance $G^{\sigma} \equiv G_{ns}^{\sigma}/G_{nn}^{\sigma}$. We assume the barrier strength equal to $Z = 0$ (contact limit), $Z = 0.5$ (intermediate limit), and $Z = 5$ (tunneling limit). The case of $Z = 5$ reflects not only the situation for planar NSJ with a thick insulating layer, but also that encountered in scanning tunneling spectroscopy (STS) experiments.[71]

Our goal in the following is to identify generic, *model-independent* features of the strongly correlated situation (i.e., with SDM). Namely, those features should not depend on the assumed dispersion relation or the pairing-potential strength.

A. *s*-wave pairing symmetry

In Fig. 5, the conductance for the s-wave gap symmetry and $\mathbf{Q}$ vector oriented perpendicular to the junction, is presented. It can be seen that there are peaks in the conductance originating from AR processes of quasiparticles having different spins, which take place when the energy E of the incoming electron fits into the so-called Andreev window (AW), see Refs. 39 (Fig. 3), 40, and 58 (Chap. 5, Figs. 5.1d and 5.4b) for more details. These peaks are separated by a distance equal to twice the Zeeman energy ($2h = g\mu_B H$) only in the case without strong correlations (SIM). For the SDM case, the correlations compensate the Zeeman splitting (by means of h_{cor} and m_{σ}, cf. Refs. 31 and 32), and as result, the conductance peaks are closer than twice the Zeeman energy. We identify this feature as a *hallmark of strong correlations in the SC state*. Another interesting feature differentiating the SIM and SDM cases is the absence of the $\sigma = \uparrow$ peak for the SDMs when the magnetic field $H \gtrsim 12$ T. For such fields, the junction is transparent for incoming particles with $\sigma = \uparrow$ because the AW[39,40] falls below $E = 0$. In other words, the quasiparticle energy $E_{\mathbf{k}+}$ within the FF SC is below zero around the whole Fermi surface. This leads to breaking of Cooper pairs and produces a NS region filling the whole angular space around the Fermi surface [see Fig. 4(b), SDM case]. Since there are normal particles with $\sigma = \uparrow$ within the FF SC, the incoming $\sigma = \uparrow$ quasiparticle does not feel the SC gap presence, and the junction is transparent, which yields $G_{\uparrow} \approx 1$.

In all the following figures, the parallel orientation of the $\mathbf{Q}$ vector with respect to the NSJ interface has been assumed. In Fig. 6, the NSJ conductance for the s-wave gap symmetry has been presented. Again, at high magnetic fields $H \gtrsim 12$ T, the junction is transparent for incoming quasiparticles with $\sigma = \uparrow$. In the present case, it is difficult to discern characteristic features of the conductance from the spin-up and spin-down channels in such a manner that the splitting of the peaks could be measured. For this purpose, the spin-resolved signals G_{σ} would have to be singled out, as shown in Figs. 6(b) and 6(d) because the spin-specific features of the total conductance are subtle and could be smeared out at finite temperatures or due to other effects (e.g., inelastic scattering). Again, the characteristic features of spin-up and spin-down signals are separated by a distance equal to twice the Zeeman energy for SIMs [Fig. 6(a)] and are closer for SDMs [Fig. 6(d)].

B. *d*-wave pairing symmetry

In Fig. 7, the conductance in the case of the FF state with $\theta_{\mathbf{Q}} = 0$ is presented. Such a phase is stable in the high-field regime (see Figs. 1 and 2). Note that, by fixing the direction of $\mathbf{Q}$ with respect to the NSJ interface, we fix also angle α (see Fig. 3), as $\theta_{\mathbf{Q}}$ is determined from the results presented in Sec. II. Namely, the parallel vector $\mathbf{Q}$ orientation with respect to the junction interface implies that $\alpha = 0$ for $\theta_{\mathbf{Q}} = 0$ [cf. Fig. 3(b)] and $\alpha = \pi/4$ for $\theta_{\mathbf{Q}} = \pi/4$ [cf. Fig. 3(c)]. In the case with $\theta_{\mathbf{Q}} = 0$, no remarkable model-independent differences between the SDM and the SIM cases appear, as all peaks present in Fig. 7 come from $\sigma = \downarrow$ electrons [see Fig. 7(a), where the $\sigma = \uparrow$ signal has been plotted].

The conductance spectra for the d-wave FF phase with $\theta_{\mathbf{Q}} = \pi/4$ (with $\alpha = \pi/4$) have been presented in Fig. 8. As in the s-wave case, and for the same reasons, at high magnetic fields, the junction is transparent for spin-up quasiparticles in the SDM case. Only at $H \lesssim 14.4$ T, were we able to discern characteristic spin-specific features of the spectra [see Figs. 8(a) and 8(d) for the spin-resolved spectra]. Again, these features are split by twice the Zeeman energy for the SIMs and are closer for the SDMs. To identify the spin-specific features, spin-resolved spectra have to be analyzed, as before in the s-wave case.

Finally, in Fig. 9, we show the conductance spectra for the d-wave BCS state with the (100) contact ($\alpha = 0$). In this case, in the tunneling limit ($Z = 5$), the peaks originating from the AR of quasiparticles with different spins, are most clearly visible. As previously, these peaks are split by twice the Zeeman energy for the SIMs and are closer for the SDMs. We identify this case as the most promising for experimental verification, as discussed in the following.

V. RELATION TO EXPERIMENT

Our results imply that the splitting between the spin-up and the spin-down features of the conductance spectra is equal to twice the Zeeman energy only in the noncorrelated case (SIM). In the strongly correlated case, due to the presence of SDMs m_σ and correlation field h_{cor}, the separation of the spin-up and the spin-down features differs essentially. In the present case of a two-dimensional correlated electron gas, this separation is smaller (because m_σ and h_{cor} compensate the Zeeman term; typically $h_{\mathrm{cor}} \approx 0.5 \times (-h)$, cf. Refs. 31 and 32), but, in general, it may be larger. For example, in the two-dimensional Hubbard model, our recent calculations[54] typically yield $h_{\mathrm{cor}} \approx 5 \times h$, and therefore, in that model, correlations *enhance* splitting of the conductance peaks.

In principle, it should be possible to measure the conductance-peaks splitting experimentally. Especially, the BCS case with the (100) contact and high barrier strength Z [Figs. 9(c) and 9(f)] looks promising, as the peaks are clearly visible, and the BCS state exists in lower magnetic fields than the FFLO state, which should make the whole analysis simpler (the orbital effects,[72] which may be essential especially on the normal-metal side, are less important in that regime).

Another feature differentiating the SIM case from the SDM situation is the absence of the spin-up features of conductance spectra for high magnetic fields and for the FF state. It is difficult to say if this feature is model independent or characteristic to the model with the dispersion relation of a free-electron gas with renormalized masses.

AR spectroscopy in magnetic fields has already been reported in a few compounds.[73–77] For example, in Mo_3Sb_7, point contact AR spectroscopy leads to identification of this compound as an unconventional SC.[77] Such measurements have also been performed on Cd-doped $CeCoIn_5$.[75,76] $CeCoIn_5$, as a heavy-fermion SC and possibly a host to the FFLO phase, is a natural candidate for verification of the present results. Spectra presented in Fig. 4 of Ref. 75 resemble our Fig. 9(e), with splitting between the spin-up and the spin-down features on the order of 8 T in fields of approximately 2 T. This might indicate that $h_{\mathrm{cor}} \uparrow\uparrow h$ (h_{cor} enhances h), but in $CeCoIn_5$, the one-band model, assumed in our calculations, may not be sufficient,[78] and therefore, our interpretation is only a speculation.[79] On the

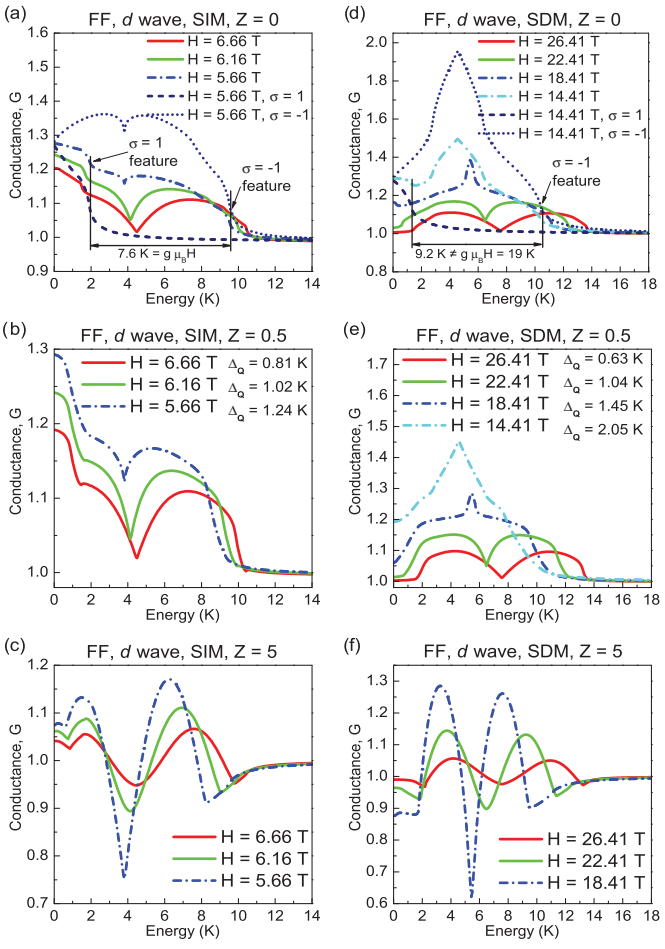

FIG. 8. (Color online) Conductance spectra for the d-wave FF state with $\theta_{\mathbf{Q}} = \pi/4$ [$\mathbf{Q}$ along the nodal direction, $\alpha = \pi/4$; cf. Figs. 2(a) and 3(c)] for selected barrier strengths for the (a)–(c) SIM and the (d)–(f) SDM cases. In (b) and (e), we provide the values of the gap $\Delta_{\mathbf{Q}}$. Also, in (a) and (d), the spin-resolved conductance G_σ has been presented to identify spectra features for both spin channels. These features are separated by twice the Zeeman energy for the SIMs and again, are closer for the SDM case.

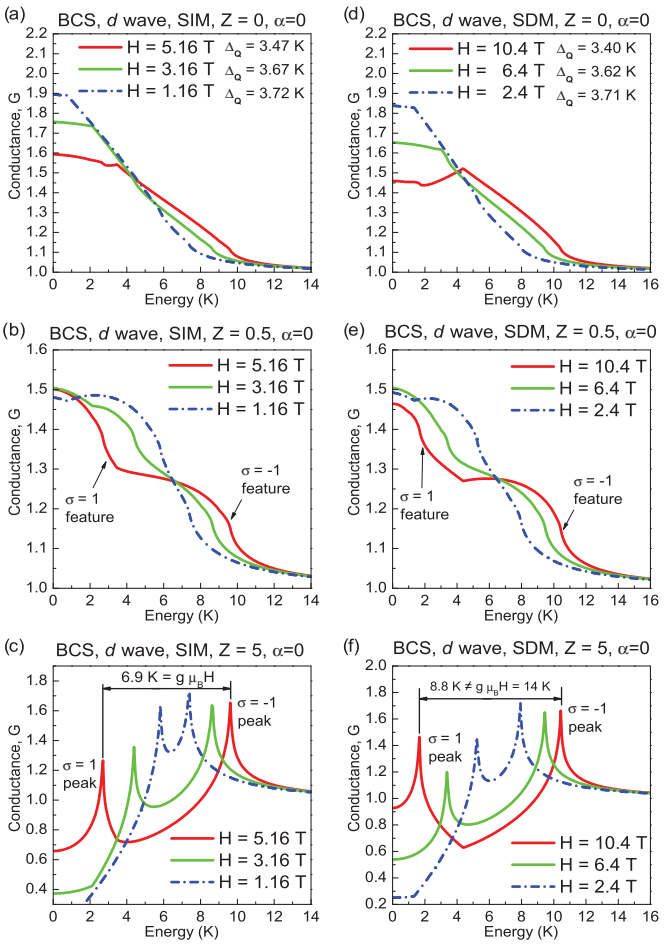

FIG. 9. (Color online) Conductance spectra for the d-wave BCS state with the (100) contact ($\alpha = 0$) for selected barrier strengths for the (a)–(c) SIM and the (d)–(f) SDM cases. In (a) and (d), we provide the values of the gap $\Delta_{\mathbf{Q}}$. In (c) and (f), in the tunneling regime ($Z = 5$), conductance peaks from spin-up and spin-down channels already are clearly visible in the total conductance G (i.e., there is no need to analyze the spin-resolved spectra G_σ). These peaks are separated by twice the Zeeman energy for (c) SIMs and are closer for (f) SDMs.

other hand, for a two-band model with strong correlations, the h_{cor} terms are also present (for both bands), and our conclusions should also hold.

Let us note that, in view of the present results, the AR spectra for the case of the BCS state with the (100) contact and in the tunneling limit (high Z) would be most helpful in detecting the effect of strong correlations in SCs. Such a configuration can be studied by both AR spectroscopy of a planar junction as well as by the STS technique.

VI. CONCLUSIONS

In this paper, we have provided a detailed analysis of the conductance spectra of a normal-metal strongly correlated SC junction. The splitting of conductance peaks in the strongly correlated case differs from that in the uncorrelated case. It is equal to twice the Zeeman energy only in the latter case, and in the correlated case, it may be smaller or larger depending on the details of the electronic structure. We identify this feature as one of the *hallmarks of strong correlations in the SC phase*, as it should hold true for other models with different dispersion relations. It is most clearly visible in the case of the BCS SC with the (100) contact and in the tunneling regime (high Z). In other cases, it also is present, but the spin-resolved conductances must be analyzed in order to identify the splitting unambiguously.

It would be interesting to examine other spectroscopic methods, such as the Josephson tunneling in the SC quantum interference device geometry for the systems with strong correlations (and specific features resulting from them: the spin-dependent masses and the correlation field). Such analysis should be carried out separately as it may lead to a decisively distinct interference pattern in an applied magnetic field.

ACKNOWLEDGMENTS

The work was supported by the Ministry of Science and Higher Education, Grants Nos. N N202 128736 and N N202 173735 as well as by the Foundation for Polish Science under the TEAM program.

*jan.kaczmarczyk@uj.edu.pl
†sadzikowski@th.if.uj.edu.pl
‡ufspalek@if.uj.edu.pl

[1] P. Fulde and R. A. Ferrell, Phys. Rev. **135**, A550 (1964).
[2] A. Larkin and Y. Ovchinnikov, J. Exp. Theor. Phys. **47**, 1136 (1964) [Sov. Phys. JETP **20**, 762 (1965)].
[3] Y. Matsuda and H. Shimahara, J. Phys. Soc. Jpn. **76**, 051005 (2007).
[4] K. Kakuyanagi, M. Saitoh, K. Kumagai, S. Takashima, M. Nohara, H. Takagi, and Y. Matsuda, Phys. Rev. Lett. **94**, 047602 (2005).
[5] K. Kumagai, M. Saitoh, T. Oyaizu, Y. Furukawa, S. Takashima, M. Nohara, H. Takagi, and Y. Matsuda, Phys. Rev. Lett. **97**, 227002 (2006).
[6] A. Bianchi, R. Movshovich, C. Capan, P. G. Pagliuso, and J. L. Sarrao, Phys. Rev. Lett. **91**, 187004 (2003).
[7] K. Kumagai, H. Shishido, T. Shibauchi, and Y. Matsuda, Phys. Rev. Lett. **106**, 137004 (2011).
[8] B.-L. Young, R. R. Urbano, N. J. Curro, J. D. Thompson, J. L. Sarrao, A. B. Vorontsov, and M. J. Graf, Phys. Rev. Lett. **98**, 036402 (2007).
[9] M. Kenzelmann, T. Strässle, C. Niedermayer, M. Sigrist, B. Padmanabhan, M. Zolliker, A. D. Bianchi, R. Movshovich, E. D. Bauer, J. L. Sarrao, and J. D. Thompson, Science **321**, 1652 (2008).
[10] G. Koutroulakis, M. D. Stewart, V. F. Mitrović, M. Horvatić, C. Berthier, G. Lapertot, and J. Flouquet, Phys. Rev. Lett. **104**, 087001 (2010).
[11] R. Ikeda, Phys. Rev. B **81**, 060510 (2010).
[12] Y. Hatakeyama and R. Ikeda, Phys. Rev. B **83**, 224518 (2011).
[13] J. Singleton, J. A. Symington, M.-S. Nam, A. Ardavan, M. Kurmoo, and P. Day, J. Phys.: Condens. Matter **12**, L641 (2000).

[14]B. Bergk, A. Demuer, I. Sheikin, Y. Wang, J. Wosnitza, Y. Nakazawa, and R. Lortz, Phys. Rev. B **83**, 064506 (2011).
[15]K. Cho, B. E. Smith, W. A. Coniglio, L. E. Winter, C. C. Agosta, and J. A. Schlueter, Phys. Rev. B **79**, 220507 (2009).
[16]P. Javorský, E. Colineau, F. Wastin, F. Jutier, J.-C. Griveau, P. Boulet, R. Jardin, and J. Rebizant, Phys. Rev. B **75**, 184501 (2007).
[17]J. K. Dong, H. Zhang, X. Qiu, B. Y. Pan, Y. F. Dai, T. Y. Guan, S. Y. Zhou, D. Gnida, D. Kaczorowski, and S. Y. Li, e-print arXiv:1008.0679.
[18]C. Pfleiderer, Rev. Mod. Phys. **81**, 1551 (2009).
[19]K. Cho, H. Kim, M. A. Tanatar, Y. J. Song, Y. S. Kwon, W. A. Coniglio, C. C. Agosta, A. Gurevich, and R. Prozorov, Phys. Rev. B **83**, 060502 (2011).
[20]R. Casalbuoni and G. Nardulli, Rev. Mod. Phys. **76**, 263 (2004).
[21]K. Machida, T. Mizushima, and M. Ichioka, Phys. Rev. Lett. **97**, 120407 (2006).
[22]J. Kinnunen, L. M. Jensen, and P. Törmä, Phys. Rev. Lett. **96**, 110403 (2006).
[23]T. K. Koponen, T. Paananen, J.-P. Martikainen, M. R. Bakhtiari, and P. Törmä, New J. Phys. **10**, 045014 (2008).
[24]A. McCollam, S. R. Julian, P. M. C. Rourke, D. Aoki, and J. Flouquet, Phys. Rev. Lett. **94**, 186401 (2005).
[25]J. Spałek and P. Gopalan, Phys. Rev. Lett. **64**, 2823 (1990).
[26]P. Korbel, J. Spałek, W. Wójcik, and M. Acquarone, Phys. Rev. B **52**, R2213 (1995).
[27]J. Spałek and W. Wójcik, *Spectroscopy of the Mott Insulators and Correlated Metals*, edited by A. Fujimori and Y. Tokura, Vol. 119 (Springer-Verlag, Berlin, 1995), pp. 41–65.
[28]J. Bauer and A. C. Hewson, Phys. Rev. B **76**, 035118 (2007).
[29]S. Onari, H. Kontani, and Y. Tanaka, J. Phys. Soc. Jpn. **77**, 023703 (2008).
[30]SDMs have also been observed in other heavy-fermion systems.[80,81] One should note at the outset that, by spin-dependent masses (or their enhancement), we understand a **k**-independent feature of a very narrow band, which is derived solely from the effect of correlation. The ordinary splitting into spin sub-bands in the Zeeman field is a separate effect.
[31]J. Kaczmarczyk and J. Spałek, Phys. Rev. B **79**, 214519 (2009).
[32]J. Kaczmarczyk and J. Spałek, J. Phys.: Condens. Matter **22**, 355702 (2010).
[33]M. M. Maśka, M. Mierzejewski, J. Kaczmarczyk, and J. Spałek, Phys. Rev. B **82**, 054509 (2010).
[34]J. Kaczmarczyk, J. Jędrak, and J. Spałek, Acta Phys. Pol. A **118**, 261 (2010).
[35]Z.-J. Ying, M. Cuoco, C. Noce, and H.-Q. Zhou, Phys. Rev. B **78**, 104523 (2008).
[36]A. Andreev, Zh. Eksp. Teor. Fiz. **46**, 1823 (1964) [Sov. Phys. JETP **19**, 1228 (1964)].
[37]G. E. Blonder, M. Tinkham, and T. M. Klapwijk, Phys. Rev. B **25**, 4515 (1982).
[38]Q. Cui, C.-R. Hu, J. Y. T. Wei, and K. Yang, Phys. Rev. B **73**, 214514 (2006).
[39]J. Kaczmarczyk, M. Sadzikowski, and J. Spałek, Physica C **471**, 193 (2011).
[40]T. Partyka, M. Sadzikowski, and M. Tachibana, Physica C **470**, 277 (2010).
[41]Y. Tanaka, Y. Asano, M. Ichioka, and S. Kashiwaya, Phys. Rev. Lett. **98**, 077001 (2007).
[42]D. Zhang, C. S. Ting, and C.-R. Hu, Phys. Rev. B **70**, 172508 (2004).
[43]V. Lukic and E. J. Nicol, Phys. Rev. B **76**, 144508 (2007).
[44]Y. Tanaka and S. Kashiwaya, Phys. Rev. Lett. **74**, 3451 (1995).
[45]C. Bruder, Phys. Rev. B **41**, 4017 (1990).
[46]S. Kashiwaya and Y. Tanaka, Rep. Prog. Phys. **63**, 1641 (2000).
[47]K. Argyropoulos and A. Dimoulas, Physica C **405**, 77 (2004).
[48]K. Maki, Phys. Rev. **148**, 362 (1966).
[49]W. K. Park and L. H. Greene, J. Phys.: Condens. Matter **21**, 103203 (2009).
[50]G. Goll, Adv. Solid State Phys. **45**, 213 (2005).
[51]G. Deutscher and P. Nozières, Phys. Rev. B **50**, 13557 (1994).
[52]M. A. N. Araújo and P. D. Sacramento, Phys. Rev. B **77**, 134519 (2008).
[53]M. A. N. Araújo and A. H. Castro Neto, Phys. Rev. B **75**, 115133 (2007).
[54]J. Jędrak, J. Kaczmarczyk, and J. Spałek, e-print arXiv:1008.0021.
[55]Q.-H. Wang, Z. D. Wang, Y. Chen, and F. C. Zhang, Phys. Rev. B **73**, 092507 (2006).
[56]K.-Y. Yang, W. Q. Chen, T. M. Rice, M. Sigrist, and F.-C. Zhang, New J. Phys. **11**, 055053 (2009).
[57]J. Spałek, Phys. Rev. B **38**, 208 (1988); J. Spałek and P. Gopalan, J. Phys. (France) **50**, 2869 (1989); J. Karbowski and J. Spałek, Phys. Rev. B **49**, 1454 (1994).
[58]J. Kaczmarczyk, Ph. D. thesis, Jagiellonian University, Kraków, 2011 [http://th-www.if.uj.edu.pl/ztms/download/phdTheses/Jan_Kaczmarczyk_doktorat.pdf].
[59]C. Petrovic, P. G. Pagliuso, M. F. Hundley, R. Movshovich, J. L. Sarrao, J. D. Thompson, Z. Fisk, and P. Monthoux, J. Phys.: Condens. Matter **13**, L337 (2001).
[60]H. Shimahara, Phys. Rev. B **50**, 12760 (1994).
[61]M. Galassi, J. Davies, J. Theiler, B. Gough, G. Jungman, P. Alken, M. Booth, and F. Rossi, *GNU Scientific Library Reference Manual*, 3rd ed. (Network Theory, Ltd., London, 2009).
[62]P. G. de Gennes, *Superconductivity of Metals and Alloys* (Westview, Boulder, CO, 1999).
[63]M. G. Burt, Phys. Rev. B **50**, 7518 (1994).
[64]N. A. Mortensen, K. Flensberg, and A.-P. Jauho, Phys. Rev. B **59**, 10176 (1999).
[65]G. Annunziata, M. Cuoco, C. Noce, A. Romano, and P. Gentile, Phys. Rev. B **80**, 012503 (2009).
[66]G. Annunziata, M. Cuoco, P. Gentile, A. Romano, and C. Noce, Phys. Rev. B **83**, 094507 (2011).
[67]G. Annunziata, H. Enoksen, J. Linder, M. Cuoco, C. Noce, and A. Sudbø, Phys. Rev. B **83**, 144520 (2011).
[68]Boundary conditions with different masses have been used before, e.g., in Refs. 65–67.
[69]These equations are written for $y = 0$. If $y \neq 0$ additional terms $e^{\pm iq_y y}$ appear but do not alter the solution, they are usually omitted for clarity.
[70]S. Chaudhuri and P. F. Bagwell, Phys. Rev. B **51**, 16936 (1995).
[71]I. Giaever, Phys. Rev. Lett. **5**, 147 (1960); M. Eschrig, C. Iniotakis, and Y. Tanaka, e-print arXiv:1001.2486; O. Fischer, M. Kugler, I. Maggio-Aprile, C. Berthod, and C. Renner, Rev. Mod. Phys. **79**, 353 (2007).
[72]P. A. M. Benistant, H. van Kempen, and P. Wyder, Phys. Rev. Lett. **51**, 817 (1983); Y. Takagaki, Phys. Rev. B **57**, 4009 (1998); Y. Asano, *ibid.* **61**, 1732 (2000); H. Hoppe, U. Zülicke, and G. Schön, Phys. Rev. Lett. **84**, 1804 (2000).

[73]T. D. Moore and D. A. Williams, Phys. Rev. B **59**, 7308 (1999).
[74]J. Kačmarčík, P. Szabó, P. Samuely, K. Flachbart, A. Nader, and A. Briggs, Physica B **259-261**, 985 (1999).
[75]W. K. Park, J. L. Sarrao, J. D. Thompson, L. D. Pham, Z. Fisk, and L. H. Greene, Physica B **403**, 731 (2008).
[76]W. K. Park, L. D. Pham, A. D. Bianchi, C. Capan, Z. Fisk, and L. H. Greene, J. Phys.: Conf. Ser. **150**, 052208 (2009).
[77]V. Dmitriev, L. Rybaltchenko, E. Khristenko, L. Ishchenko, Z. Bukowski, and R. Troć, Acta Phys. Pol. A **114**, 263 (2008).
V. Dmitriev, L. Rybaltchenko, L. Ishchenko, E. Khristenko, Z. Bukowski, and R. Troć, Low Temp. Phys. **33**, 1009 (2007).
[78]M. Fogelström, W. K. Park, L. H. Greene, G. Goll, and M. J. Graf, Phys. Rev. B **82**, 014527 (2010).
[79]Additionally, in the aforementioned Fig. 4 of Ref. 75, antiferromagnetism also plays a role in the presented spectra.
[80]I. Sheikin, A. Gröger, S. Raymond, D. Jaccard, D. Aoki, H. Harima, and J. Flouquet, Phys. Rev. B **67**, 094420 (2003).
[81]M. Takashita, H. Aoki, T. Terashima, S. Uji, K. Maezawa, R. Settai, and Y. Ōnuki, J. Phys. Soc. Jpn. **65**, 515 (1996).